17th World Conference on Earthquake Engineering, 17WCEE
Sendai, Japan - September 13th to 18th 2020

MAINSHOCK-AFTERSHOCK DAMAGE ASSESSMENT OF CONCRETE BRIDGE REINFORCED WITH SHAPE MEMORY ALLOY REBAR

AHMM. Billah[1] and B. Todorov [2]

[1] *Assistant Professor, Department of Civil Engineering, Lakehead University, muntasir.billah@lakeheadu.ca*
[2] *Graduate Research Assistant, Department of Civil Engineering, Lakehead University, btodorov@lakeheadu.ca*

Abstract

Shape memory alloy (SMA) has emerged as an alternative to conventional steel reinforcement for improving the seismic performance of bridges during an extreme earthquake. However, mainshock and aftershock seismic sequences can lead to severe damage accumulation and strength degradation to structures resulting in extensive required repairs or even collapse. No study has been performed to evaluate the efficacy of SMA reinforced concrete bridge pier under MS-AS sequence. Therefore, the seismic fragility of SMA-RC piers can be significantly underestimated if the hazard characterization considers only mainshock earthquake events and triggered aftershock events are neglected. The objective of this study is to evaluate the seismic fragility of concrete bridge piers reinforced with two different types of SMA (e.g. Ni-Ti and Fe-based) rebars under mainshock ground motions followed by aftershocks. Using incremental dynamic analysis and probabilistic seismic demand models, the fragility curves of the SMA-RC bridge piers under main shock alone and MS-AS sequence have been developed and compared against conventional steel reinforced concrete bridge piers. Considering residual drift as demand parameters, fragility curves are developed for different SMA-RC bridge piers. The outcome of this study demonstrates the effect of aftershocks on SMA-RC bridge pier.

Keywords: Performance-based design; Shape Memory Alloy; Bridge pier; Seismic performance.

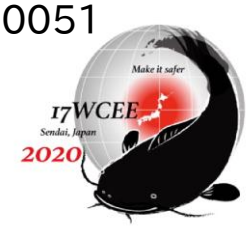

1. Introduction

Current seismic design codes and assessment guidelines only consider mainshock events for new design and assessment of existing structures. However, aftershock events can cause severe damage to buildings and bridges thus increasing the risk of structural collapse and life safety. Although aftershocks are usually smaller in magnitude, they can have longer duration, different intensity and frequency content from the mainshock [1]. Most of the recent major earthquakes around the world, for example L'Aquila, Italy 2009, Chile 2012, Christchurch, New Zealand, 2011–2012, and Tohoku, Japan, 2011, were followed by aftershock events which showed that structures are more vulnerable to severe damage and collapse under mainshock-aftershock (MS-AS) sequence. More than 80,000 aftershocks were recorded in the Ridgecrest area after the 2019 Ridgecrest earthquake in California. Observations from recent earthquakes have shown that, when subjected to aftershocks, structures can experience greater damage as a result of significant reduction of stiffness and strength in structural components from mainshocks [2].

There is a growing interest of assessing the performance of structures when subjected to sequence of MS-AS [3-5]. However, most of the studies are focused on buildings and very few are focused on bridges [6,7]. Yet, the post-earthquake functionality of bridges is very important to ensure mobility of emergency vehicles for rescue and emergency operations. Nevertheless, past experiences have shown that bridges undergoing large lateral drift are prone to large residual deformation which can significantly increase under MS-AS sequence. Over the last few years, researchers have experimentally and numerically investigated the potential application of shape memory alloys in bridge piers and found promising results [8,9] in reducing the residual drift of bridge piers. No study has been performed to evaluate the efficacy of SMA reinforced concrete bridge pier under MS-AS sequence. Therefore, the seismic performance of SMA-RC piers can be significantly underestimated if the hazard characterization considers only mainshock events and triggered aftershock events are neglected. The objective of this study is to evaluate the seismic fragility of concrete bridge piers reinforced with two different types of SMA (e.g. Ni-Ti and Fe-based) rebars under mainshock ground motions followed by aftershocks. The seismic fragility of the SMA-RC bridge piers is compared with conventional steel-reinforced concrete (Steel-RC) bridge piers. This study provides a preliminary attempt to investigate the efficacy of SMA-RC bridge piers when subjected to MS-AS sequence and compare the seismic vulnerability with conventional bridge piers.

2. Methodology

This section provides a detailed description for developing fragility curves for mainshock-damaged SMA-RC and Steel-RC bridge piers. The first step involves developing the fragilities for as-built SMA-RC bridge piers and the next step describes how the fragility curves for mainshock damaged bridge piers were developed.

2.1 Fragility Curve for Bridge Pier under Mainshock

In this study, the fragility curves for the as-built bridge piers for mainshock events are developed using a probabilistic seismic demand model (PSDM) and limit state model. The PSDM which relates the median demand to the intensity measure (IM) is developed using the results obtained from IDA and the power law function [10]. The PSDM provides a logarithmic correlation between median demand and the selected IM:

$$EDP = a(IM)^b \tag{1}$$

In the log transformed space, Equation 1 can be expressed as

$$\ln(EDP) = \ln(a) + b\ln(IM) \tag{2}$$

Where, a and b are unknown coefficients which can be estimated from a regression analysis of the response data collected from IDA. Effectiveness of a demand model is determined by the ability of

evaluating Equation 2 in a closed form. In order to accomplish this task, it is assumed that the EDPs follow log-normal distributions. The dispersion ($\beta_{EDP|IM}$) accounting for the uncertainty in the relation which is conditioned upon the IM, is estimated using Equation 3 [11]:

$$\beta_{EDP|IM} = \sqrt{\frac{\sum_{i=1}^{N}\left(\ln(EDP) - \ln\left(aIM^{b}\right)\right)^{2}}{N-2}} \tag{3}$$

Where, N is the number of simulations. With the probabilistic seismic demand models and the limit states corresponding to various damage states, it is now possible to generate fragilities (i.e. the conditional probability of reaching a certain damage state for a given IM) using Equation 4 [12].

$$P[DS \mid IM] = \phi\left[\frac{\ln(IM) - \ln(IM_n)}{\beta_{comp}}\right] \tag{4}$$

Φ[.] is the standard normal cumulative distribution function and

$$\ln(IM_n) = \frac{\ln(S_c) - \ln(a)}{b} \tag{5}$$

$\ln(IM_n)$ is defined as the median value of the intensity measure for the chosen damage state, a and b are the regression coefficients of the PSDMs, and the dispersion component is presented in Equation 6 [12].

$$\beta_{comp} = \frac{\sqrt{\beta_{EDP|IM}^2 + \beta_c^2}}{b} \tag{6}$$

2.2 Fragility Curve for Bridge Pier under Aftershock

Fragility curves for the bridge piers for aftershock events are also developed using a probabilistic seismic demand model (PSDM) and limit state model. However, mainshock fragility describes the conditional probability of damage considering a mainshock intensity measure while the aftershock fragility is developed as a conditional probability that determines the likelihood that a mainshock damaged pier will meet or exceed a certain damage level, given an aftershock intensity measure (IMAS) and an initial damage state (IDS) associated with the mainshock. Aftershock fragility curves are associated with the damage accumulated during the mainshock event and reflect the increased vulnerability of structures. Equations 1 through 6 are also used for aftershock fragility assessment of the SMA-RC and Steel-RC bridge piers.

3. Design of Bridge Piers

In this study two concrete bridge piers reinforced with two different SMAs are designed following the performance-based design guidelines proposed by Billah and Alam [13]. The bridge piers are assumed to be located at Vancouver, BC with the site soil class-C (stiff soil). The corresponding design spectrum is selected, with a 2% probability of exceedance in 50 years that corresponds to a return period of 2475 year, according to the CHBDC-2014 [14]. The bridge is considered to be a lifeline bridge according to the bridge classification described in CHBDC-2014. For the selected seismic hazard level (2% in 50 years), the bridge should be operational (repairable damage) with limited service to meet the performance requirements. In addition, a conventional bridge pier reinforced with steel rebar is also designed following CHBDC-2014 and similar design criteria and performance requirement.

The height and diameter of all the bridge piers are assumed to be 5m and 1m, respectively. Two different SMAs having different combinations of alloys and mechanical properties are selected which are shown in Table 1. The material properties of concrete and steel reinforcement are listed in Table 2. The final design yielded all the bridge piers to be reinforced with 28 longitudinal SMA rebars of different diameter in the plastic hinge region and the remaining portion was reinforced with 28-25M steel (diameter 25.2 mm) rebar. To meet the current seismic design requirements, shear reinforcement was provided using 15 mm spirals at 50 mm pitch. The bridge piers are specified as SMA-RC-1 (reinforced with SMA-1), SMA-RC-2 (reinforced with SMA-2), and Steel-RC (reinforced with steel rebar). SMA-RC-1 is reinforced with 28-25 mm SMA-1 and SMA-RC-2 is reinforced with 28-22.5 mm SMA-2 bars in the plastic hinge region. Fig. 1 shows the cross section and elevation of the bridge pier. In this study, the plastic hinge length of the SMA-RC bridge piers are calculated using the plastic hinge expression (Equation 7) proposed by Billah and Alam [15].

$$\frac{L_p}{d} = 1.05 + \left(0.25\frac{P}{f_c' A_g}\right) + \left(0.08\frac{L}{d}\right) + \left(0.0002 f_{y-SMA}\right) - (0.16\rho_l) - (0.019 f_c') - (0.24\rho_s) \quad (1)$$

Where L_p is the plastic hinge length, d is the diameter of the pier, L/d is the aspect ratio, $P/f_c' A_g$ is the axial load ration, ρ_l = longitudinal reinforcement ratio, ρ_s = transverse reinforcement ratio, f_{y-SMA} = yield strength of SMA rebar and f_c' = concrete compressive strength. This equation showed reasonable accuracy in predicting the plastic hinge length measured from experimental investigations. The bridge piers are modeled using a fiber based finite element program Seismostruct [16] to explicitly model the concrete, SMA and reinforcing steel materials. Details of the bridge pier modeling can be found in Billah and Alam [17].

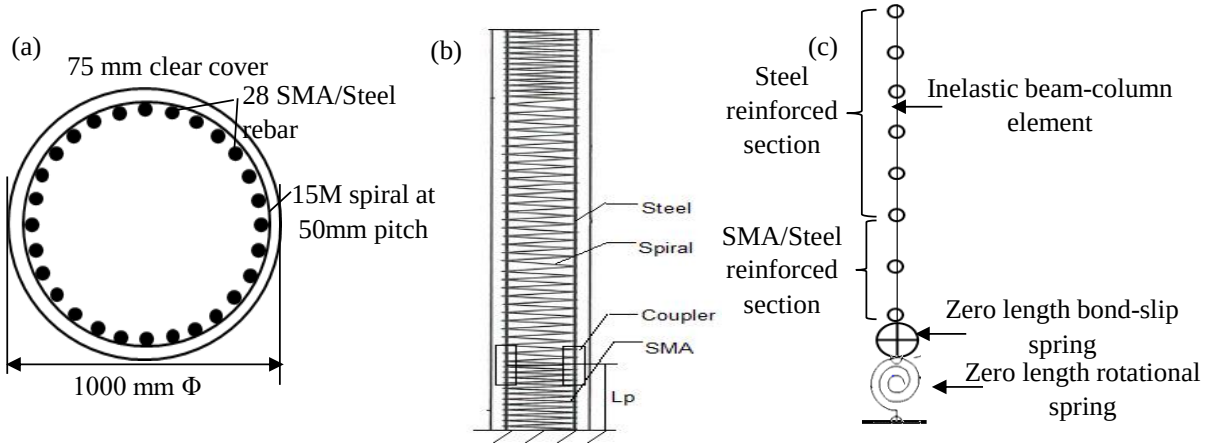

Fig. 1 – (a) Cross section, (b) elevation and (c) finite element model of SMA-RC bridge pier

Table 1 – Properties of different types of SMA

Alloy	SMA ID	E (GPa)	ε_s (%)	f_y (MPa)	f_{p1} (MPa)	f_{T1} (MPa)	f_{T2} (MPa)	Ref
$NiTi_{45}$	SMA-1	62.5	6	401.0	510	370	130	Alam et al. [18]
FeNCATB	SMA-3	46.9	13.5	750	1200	300	200	Tanaka et al. [19]

f_y (austenite to martensite starting stress); f_{P1}(austenite to martensite finishing stress); f_{T1}(martensite to austenite starting stress); f_{T2}(martensite to austenite finishing stress), ε_s (maximum superelastic strain); and E (modulus of elasticity)

Table 2 – Material properties for SMA-RC bridge pier

Material	Property	
Concrete	Compressive Strength (MPa)	42.4
	Corresponding strain	0.0029
	Tensile strength (MPa)	3.5
	Elastic modulus (GPa)	23.1
Steel	Elastic modulus (GPa)	200
	Yield stress (MPa)	475
	Ultimate stress (MPa)	692
	Ultimate strain	0.14
	Plateau strain	0.016

4. Mainshock-Aftershock Ground Motions

For seismic fragility assessment, selection of appropriate ground motions which are representatives of the seismic hazard of the site under consideration is very important. In this study, the ground motion records are selected for bridge piers located in site soil class-C (V_{S30} = 550 m/s), in Vancouver, BC, Canada. For the seismicity in Vancouver, consideration of shallow crustal, subcrustal, and mega-thrust Cascadia subduction events are important since they have very different event and ground motion characteristics due to different source and path effects [20]. In this study, the ground motions are selected by developing conditional mean spectrums (CMS) for the three different earthquake scenarios (crustal, inslab and interface) that significantly contribute to the seismic hazard of Vancouver. The CMS for three different earthquake events are developed following the method described in Baker et al. [21]. In this study 30 ground motion suits (10 from each earthquake scenario) are selected for both mainshock and aftershock records that represent crustal, inslab, and interface earthquakes in the site under consideration.

5. Mainshock Fragility Curves

Incremental Dynamic Analyses (IDAs) are performed using the selected 30 mainshock earthquake records for the SMA-RC and steel-RC bridge piers. In this study, residual drift is considered as the engineering demand parameter (EDP) and peak ground acceleration (PGA) is considered as the intensity measure for developing the fragility curves. The residual drifts monitored from IDA are incorporated into a PSDM which establishes a linear regression of demand (EDP)–intensity measure (IM) pairs in the log-transformed space. This linear regression model is used to determine the slope, intercept, and dispersion of the EDP-IM relationship. Based on the residual drift damage states proposed by Billah and Alam [22], it was assumed that a residual drift below 0.25% would meet the serviceability requirement providing full functionality while a residual drift larger than 1% would be characterized as a collapse damage state since major repair or even demolition of the structure would be needed. Using equations 1 to 6, fragility curves for the three bridge piers are developed as shown in Fig. 2. The evaluation of the fragilities (shown in Fig. 2) for residual drift indicates that for all the damage states from slight to collapse, the steel-RC bridge pier possesses more vulnerability as compared to the SMA-RC bridge piers. A closer look into Fig. 2 reveals that, at all damage states SMA-RC-2 has lower probability of exceeding a certain damage level. This can be attributed to the higher superelastic strain of SMA-3, which allowed higher recentering of SMA-RC-3 thus resulting in lower residual drift.

Table 3 – Selected earthquake ground motion records

No	Eq. Name	Record ID	Event ID	Type	Mw	Epi. Dis (km)	PGA (g)	PGV (cm/s)	Source
1	Northridge	953	127	Crustal	6.69	17.15	0.46	54	PEER
2	Duzce, Turkey	1602	138	Crustal	7.14	12.04	0.72	59	PEER
3	Hector mine	1787	158	Crustal	7.16	11.66	0.31	34	PEER
4	Imperial Valley	169	50	Crustal	6.53	22.03	0.28	28	PEER
5	Kocaeli,Turkey	1158	136	Crustal	7.51	15.37	0.3	54	PEER
6	Landers	900	125	Crustal	7.28	23.62	0.21	38	PEER
7	Loma Prieta	752	118	Crustal	6.93	15.23	0.48	34	PEER
8	Manjil, Iran	1633	144	Crustal	7.37	12.56	0.52	47	PEER
9	Chi Chi, Taiwan	1485	137	Crustal	7.62	26	0.47	39	PEER
10	Kobe, Japan	1106	129	Crustal	6.9	0.96	0.71	78	PEER
11	Tohoku, Japan	27538	368	Inslab	6.8	111.88	0.85	23	K-KIK
12		27451	368	Inslab	6.8	114.01	0.48	16	K-KIK
13		27454	368	Inslab	6.8	112.09	0.48	12	K-KIK
14		9813	184	Inslab	7	117.21	0.75	19	K-KIK
15		9837	184	Inslab	7	52.16	0.72	15	K-KIK
16		9831	184	Inslab	7	79.59	0.58	20	K-KIK
17		20480	294	Inslab	6	52.26	0.15	13	K-KIK
18		19650	285	Inslab	6.2	79.79	0.14	10	K-KIK
19	Tokachi-oki, Japan	6306	148	Inslab	6.8	58.31	0.41	33	K-KIK
20		6267	141	Inslab	6.8	46.89	0.39	25	K-KIK
21	Tokachi-oki, Japan	19085	276	Interface	7	76.98	0.66	24.60	K-KIK
22		19004	276	Interface	7	93.02	0.34	20.18	K-KIK
23		11026	194	Interface	7.9	119.95	0.56	36.6	K-KIK
24		11025	194	Interface	7.9	62.65	0.38	60.15	K-KIK
25		21598	301	Interface	7.1	97.14	0.38	13.28	K-KIK
26	Tohoku, Japan	169	-	Interface	9	83.70	1.75	7.090	K-KIK
27		175	-	Interface	9	71	0.96	44.43	K-KIK
28		237	-	Interface	9	69.14	0.90	56.84	K-KIK
29		323	-	Interface	9	62.49	0.67	27.09	K-KIK
30		168	-	Interface	9	66.35	0.62	28.47	K-KIK

6. Aftershock Fragility Curves

In order to perform IDA for a mainshock-damaged bridge pier, a sequence of mainshock and aftershock records was entered into the model. For a given sequence of mainshock and aftershock records, the scale factor for a given mainshock response was unchanged while the intensity of the aftershock record was scaled until the model collapsed. For the effect of aftershock analysis, five different damage scenarios accumulated during mainshock event were considered. The mainshock induced damage considered in this study corresponding to maximum residual drifts are: no initial damage (DS0), 0.2% (DS1), 0.3% (DS2), 0.4% (DS3), and 0.5% (DS4). For each pair of aftershock motion-bridge pier, IDA was performed, and the maximum residual drift was monitored. Considering a lognormal distribution of seismic demand, a linear regression of the demand-intensity measure pairs in the log-transformed space, the so-called probabilistic seismic demand model (PSDM) was developed for each bridge pier. As indicated by the closed form of fragility function in Equation 4, a reliable capacity limit state model is required for developing dependable fragility curves. For the selected demand parameters, each limit state model is assumed to follow a two-parameter lognormal distribution (median S_C and dispersion β_C).

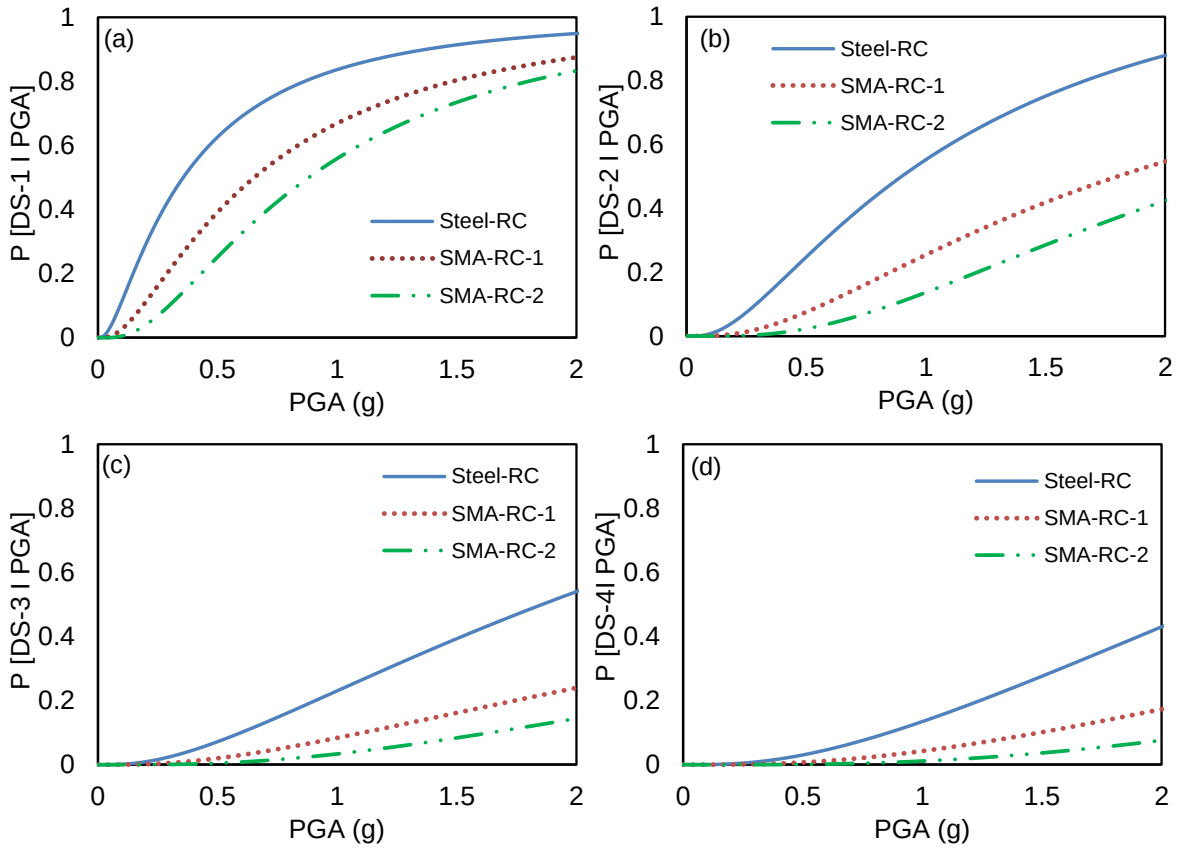

Fig. 2 – Mainshock fragility curves (a) slight damage, (b) moderate damage, (c) extensive damage and (d) collapse

Table 4 lists parameter values used to define the limit state models on the basis of residual drift (%). The component limit states developed by Billah and Alam [22] has been used in this study. Since the study of Billah and Alam (2016a) only provides the median values (S_C), a prescriptive approach described by Nielson (2005) is followed to define dispersions of limit state models (β_C). The dispersion values are calculated using the following equation provided by Nielson [12].

$$\beta_c = \sqrt{\ln(1 + COV^2)} \tag{2}$$

In this equation the COV values for different limit states are calculated based on the probabilistic distribution of different limit states described in Billah and Alam [22]. The COV values were found to be 0.21, 0.26, 0.45 and 0.52 for DS-1, DS-2, DS-3 and DS-4, respectively. These values yielded in similar dispersion values (βC) as described by other researchers [12].

Table 4 – Limit state capacity of SMA-RC bridge pier in terms of residual drift

Damage State	Residual Drift					
	SMA-RC-1		SMA-RC-3		Steel-RC	
	S_c	β_c	S_c	β_c	S_c	β_c
DS-1	0.33	0.21	0.33	0.21	0.25	0.25
DS-2	0.62	0.26	0.62	0.26	0.75	0.25
DS-3	0.87	0.43	0.87	0.43	1.00	0.46
DS-4	1.22	0.50	1.22	0.50	1.50	0.46

Using Eqn. 4, aftershock fragility curves were generated with the aftershock PSDMs and the capacity limit states. Figs. 3-5 illustrates the resulting aftershock fragility curves with different initial damage states for the analyzed SMA-RC and Steel-RC bridge piers.

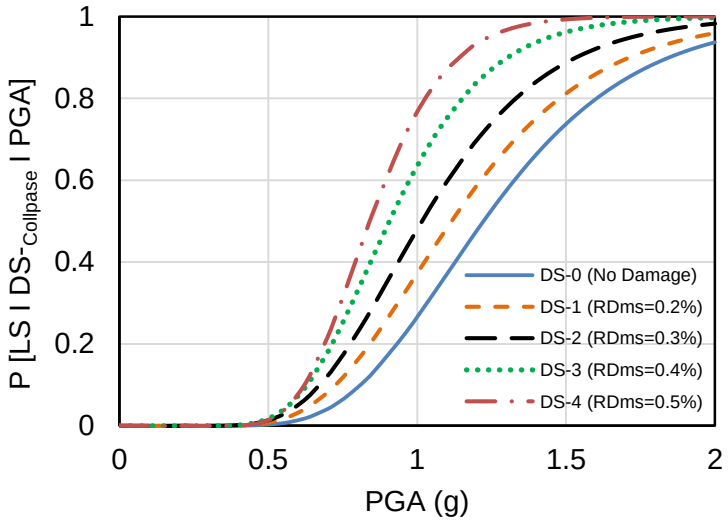

Fig. 3 – Aftershock fragility curves for SMA-RC-1 pier for collapse damage states

As presented in the figures, an aftershock fragility curve with an initially severe damage state takes on a steeper slope. This is true for all three bridge piers. For example, when SMA-RC-1 is subject to an aftershock, comparison of DS0 (undamaged) and DS4 (damaged) indicates that an aftershock would have a 44% increased probability of failure for collapse damage state, at a PGA of 1.0g. For SMA-RC-2 and Steel-RC pier, an aftershock would have a 38% and 61% increased probability of failure, respectively for collapse damage state, at a PGA of 1.0g.

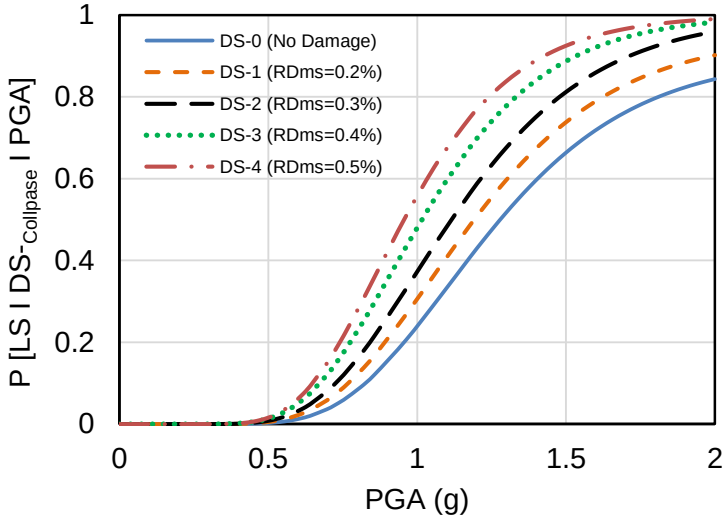

Fig. 4 – Aftershock fragility curves for SMA-RC-2 pier for collapse damage states

Therefore, given the specific intensity measure, this aftershock fragility curve conditioned on an initially severe damage state has a higher failure probability, resulting in increased vulnerability of structures subjected to multiple earthquakes. The aftershock fragility curves reveal that the Steel-RC bridge piers are more vulnerable to aftershock collapse as compared to SMA-RC bridge piers. When subjected to aftershock only (DS0), the probability of collapse of Steel-RC, SMA-RC-1 and SMA-RC-2 at PGA of 1.0 is 36%, 30%, and 22%, respectively. Bridge piers with moderate residual drift (0.3%) from mainshock have 80%, 64% and

50% probability of collapse when subjected to aftershocks for Steel-RC, SMA-RC-1, and SMA-RC-2, respectively.

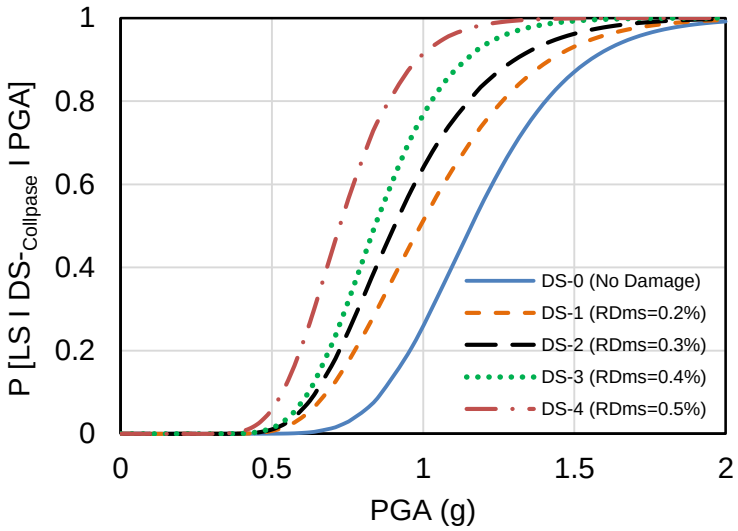

Fig. 5 – Aftershock fragility curves for Steel-RC pier for collapse damage states

7. Conclusions

In this paper, fragility curves are generated for three types of bridge piers reinforced with conventional steel rebars and two types of shape memory alloy rebars. The bridge piers are subjected to mainshock-aftershock earthquake sequences from crustal, subcrustal, and subduction zone events. The models of the bridge piers used in the analysis contain salient damage features that are capable of capturing the degradation in stiffness and strength in structural components. Aftershock PSDMs were developed in terms of a peak ground acceleration and residual drift. The PSDMs indicated that the more damage a structure initially sustains, the higher the seismic demand in subsequent earthquakes. Moreover, applying limit states and the aftershock PSDMs, aftershock fragility curves with different initial damage states were generated and compared, providing evidence that the more damage a structure initially sustains, the higher the seismic demand when the structure is subjected to same aftershock ground motions.

Comparing the fragility relationships for the three bridge piers, the following conclusions are drawn:

- Irrespective of the reinforcement configurations, all three bridge piers have a high damage potential under aftershocks than the damage potential from mainshocks. This is due to the damage induced to structures from preceding mainshocks.

- The level of damage induced from mainshock events significantly affect the aftershock vulnerability. As the damage accumulation increases from the mainshock, the probability of collapse increases under aftershock.

- Steel-RC bridge pier is more susceptible to collapse when subjected to MS-AS sequence irrespective of damage induced by mainshock event as compared to SMA-RC bridge pier.

- Irrespective of the damage accumulated from mainshock, SMA-RC-2 bridge pier was able to reduce the collapse probability under MS-AS sequence.

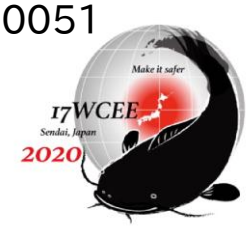

8. Acknowledgement

This study was supported by Natural Sciences and Engineering Research Council (NSERC) of Canada through Discovery Grant and Lakehead University SRC Research Development Fund (RDF). The financial support is greatly appreciated.

9. References

[1] Nazari, N,. Lindt, Jw., Li. Y. (2014). Effect of Mainshock-Aftershock Sequences on Woodframe Building Damage Fragilities, ASCE Journal of Performance of Constructed Facilities, 29(1).

[2] Abdelnaby, A. and Elnashai, A. (2014). Performance of degrading reinforced concrete frame systems under Tohoku and Christchurch earthquake sequences, J. Earthq. Engr., 18(7), 1009–1036.

[3] Abdelnaby A.E. (2017): Fragility Curves for RC Frames Subjected to Tohoku Mainshock-Aftershocks Sequences, Journal Of Earthquake Engineering, Doi: 10.1080/13632469.2016.1264328.

[4] Dong, Y. and Frangopol, DM. (2015) Risk and resilience assessment of bridges under mainshock and aftershocks incorporating uncertainties. Engineering Structures 83 (2015) 198–208.

[5] Ruiz-Garcia, J. and Aguilar, J. (2014) "Aftershock seismic assessment taking into account post-mainshock residual drifts," Journal of Earthquake Engineering and Structural Dynamics, 44(9),1391–1407.

[6] Alessandri, S., Giannini, R. and Paolacci, F. (2013) Aftershock risk assessment and the decision to open traffic on bridges, Earthquake Engng Struct. Dyn. 2013; 42:2255–2275.

[7] Fakharifar, M., Chen, G., Sneed, L., Dalvand, A., Seismic performance of post-mainshock FRP/steel repaired RC bridge columns subjected to aftershocks, Composites: Part B, 72, 183-198.

[8] Billah AHMM and Alam MS. (2014) Seismic fragility assessment of concrete bridge piers reinforced with superelastic shape memory alloy. Earthquake Spectra; DOI: 10.1193/112512EQS337M

[9] Noguez, C.A. and Saiidi, M.S. (2012). Performance of Advanced Materials during Earthquake Loading Tests of a Bridge System. J. Struct. Eng., 139, 144-154.

[10] Cornell, A.C., Jalayer, F., Hamburger, R.O. (2002). Probabilistic basis for 2000 SAC federal emergency management agency steel moment frame guidelines. J. Struct. Eng., 128, 526–532.

[11] Baker, J.W., Cornell, C.A. (2006). Vector-valued ground motion intensity measures for probabilistic seismic demand analysis. Pacific Earthquake Engineering Research report 2006/08, PEER Center, University of California Berkeley.

[12] Nielson, B.G. (2005). Analytical Fragility Curves for Highway Bridges in Moderate Seismic Zones. Ph.D. thesis, Georgia Institute of Technology, Atlanta.

[13] Billah AHMM and Alam MS. (2016). Performance-based seismic design of Shape Memory Alloy (SMA) reinforced concrete bridge pier-Part 2: Methodology and Design Example. ASCE J. Struct. Eng., 142 (12).

[14] Canadian Highway Bridge design code. (2014). CAN/CSA-S6-14. Draft version for public review. National Research Council of Canada, Ottawa; ON.

[15] Billah AHMM and Alam MS. (2016). "Plastic hinge length of shape memory alloy (SMA) reinforced concrete bridge pier." Engineering Structures, 117(2016):321-331.

[16] SeismoSoft, 2016. SeismoStruct - A computer program for static and dynamic nonlinear analysis of framed structures, V 7 [online], available from URL: www.seismosoft.com.

[17] Billah AHMM and Alam MS. (2018). "Probabilistic seismic risk assessment of concrete bridge piers reinforced with different types of shape memory alloys." Engineering Structures, 162(2018):97-108.

[18] Alam, M.S., Youssef. M.A. and Nehdi, M. (2008). "Analytical prediction of the seismic behaviour of superelastic shape memory alloy reinforced concrete elements." Engr. Struct., 30(12): 3399-3411.

[19] Tanaka, Y., Himuro, Y., Kainuma, R., Sutou, Y., Omori, T., Ishida, K. (2010). Ferrous polycrystalline shape-memory alloy showing huge superelasticity. Science, 327, 1488-1490.

[20] Goda, K., and Atkinson, G. M. (2011). Seismic performance of wood-frame houses in south-western British Columbia. Earthquake Engineering and Structural Dynamics, 40, 903–924.

[21] Baker, J. W. (2011). The conditional mean spectrum: a tool for ground motion selection. ASCE Journal of Structural Engineering, 137: 322–331.

[22] Billah AHMM and Alam MS. (2016). “Performance based seismic design of concrete bridge pier reinforced with Shape Memory Alloy- Part 1: Development of Performance- Based Damage States.” ASCE J. Struct. Eng, 142 (12).

